Applied Physics Express



# Current perpendicular to film plane type giant magnetoresistance effect using a Ag–Mg spacer and $Co_2Fe_{0.4}Mn_{0.6}Si$ Heusler alloy electrodes

Applied Physics Express **8**, 119201 (2015)
http://dx.doi.org/**10.7567/APEX.8.119201**

# Erratum: "Current perpendicular to film plane type giant magnetoresistance effect using a Ag–Mg spacer and $Co_2Fe_{0.4}Mn_{0.6}Si$ Heusler alloy electrodes" [Appl. Phys. Express 8, 063008 (2015)]

Hiroyuki Narisawa, Takahide Kubota*, and Koki Takanashi

*Institute for Materials Research, Tohoku University, Sendai 980-8577, Japan*
E-mail: tkubota@imr.tohoku.jp

Received October 13, 2015; accepted October 14, 2015; published online October 29, 2015

We had overestimated the areas of the current-perpendicular to film plane giant magnetoresistance (CPP-GMR) devices. After careful verification of the device size using the transmission electron microscopy image shown in Ref. 1, we found that the length of the device edge is about 10 nm smaller than the value used in the original paper (Ref. 2). After correcting the device size, the resistance area products ($RA$) and the values of parasitic resistance ($R_{para}$) in Fig. 3 in Ref. 2 should be changed. The specifications of the junctions in Table I in Ref. 2 should also be corrected. Finally, the values of the vertical axes should be changed for Figs. 4 and 5 in Ref. 2. Based on the above corrections, Figs. 3, 4, and 5 and Table I in Ref. 2 should be substituted by Figs. 1, 2, and 3 and Table I, respectively. These changes do not affect the discussion or conclusions in the original article.

1) H. Narisawa, T. Kubota, and K. Takanashi, Appl. Phys. Express **8**, 119102 (2015).
2) H. Narisawa, T. Kubota, and K. Takanashi, Appl. Phys. Express **8**, 063008 (2015).

**Table I.** Summary of the specifications for the junctions investigated in this study. The values without brackets are the averages for $MR_{obs}$, $MR_{int}$, and $\Delta RA$, while those values in brackets are the maximum obtained values.

| Mg content (at.%) | $RA$ (mΩ·μm$^2$) | $MR_{obs}$ (%) | $MR_{int}$ (%) | $\Delta RA$ (mΩ·μm$^2$) |
|---|---|---|---|---|
| 0 | 23 | 35 (38) | 50 (57) | 12 (13) |
| 17 | 36 | 36 (40) | 44 (49) | 16 (17) |

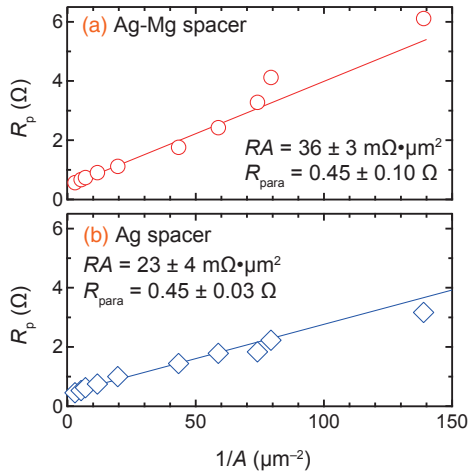


**Fig. 1.** Plots of the junction resistance at the parallel magnetization configuration ($R_p$) as a function of the inverse junction area ($1/A$) for (a) the Ag–Mg spacer and (b) the Ag spacer.

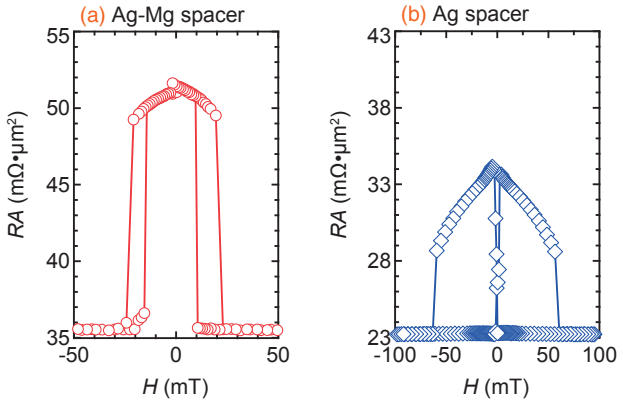


**Fig. 2.** Magnetoresistance curves of the CPP-GMR junctions using (a) the Ag–Mg spacer and (b) the Ag spacer.

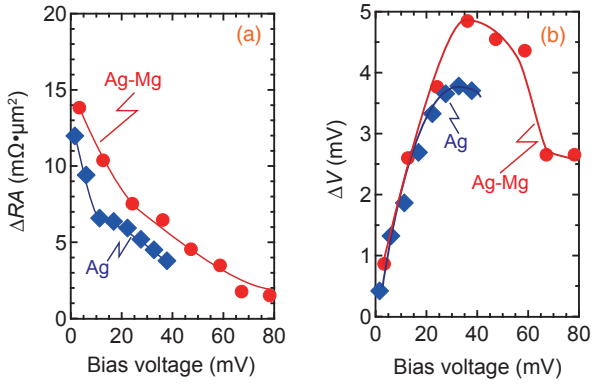


**Fig. 3.** Bias voltage dependencies of (a) the $\Delta RA$ values and (b) the output voltage $\Delta V$ of the CPP junctions. Red solid circles and blue solid diamonds represent data points for the junctions using the Ag–Mg spacer and the Ag spacer, respectively.

Applied Physics Express **8**, 063008 (2015)
http://dx.doi.org/**10.7567/APEX.8.063008**

# Current perpendicular to film plane type giant magnetoresistance effect using a Ag–Mg spacer and $Co_2Fe_{0.4}Mn_{0.6}Si$ Heusler alloy electrodes

Hiroyuki Narisawa, Takahide Kubota*, and Koki Takanashi

*Institute for Materials Research, Tohoku University, Sendai 980-8577, Japan*
E-mail: tkubota@imr.tohoku.jp

Received April 7, 2015; accepted May 3, 2015; published online May 27, 2015

The current perpendicular to film plane type giant magnetoresistance (CPP-GMR) effect in $Co_2Fe_{0.4}Mn_{0.6}Si/Ag_{83}Mg_{17}/Co_2Fe_{0.4}Mn_{0.6}Si$ junctions was investigated. An epitaxially grown 5-nm-thick $Ag_{83}Mg_{17}$ film having partially ordered $L1_2$ structure was fabricated on the $Co_2Fe_{0.4}Mn_{0.6}Si$ layer by magnetron sputtering. CPP-GMR effects were observed in the submicrometer-sized junctions, and the maximum value of the observed (intrinsic) MR ratio was 40% (48%) at room temperature. The average change in the resistance–area product was 23 mΩ·μm$^2$ for the Ag–Mg junctions, which was higher than those of conventional CPP-GMR junctions using a Ag spacer layer.


The current perpendicular to film plane type giant magnetoresistance (CPP-GMR) effect is a key technology for next-generation hard disk drives (HDDs) with an areal density of more than several terabits per square inch.[1)] To realize high-output CPP-GMR junctions, cobalt-based full Heusler alloys are promising materials because of their half-metallic electronic structure, which can generate highly spin-polarized conduction electrons.[2)] The potential of CPP-GMR junctions has been experimentally demonstrated using several cobalt-based compounds, such as $Co_2MnSi$,[3,4)] $Co_2Fe(Al\text{-}Si)$,[5,6)] $Co_2(Fe\text{-}Mn)Si$,[7,8)] and $Co_2Fe(Ge\text{-}Ga)$.[9)] The reported values of the MR ratio and the change in the resistance–area product ($\Delta RA$) were greater than 50% and 12 mΩ·μm$^2$, respectively.[8,9)] Such large values of the MR ratio and $\Delta RA$ are attributed to the half-metallic nature of Heusler alloys from fitting[9)] based on a model proposed by Valet and Fert.[10)] These studies encourage the development of CPP-GMR reading head applications for HDDs using Heusler alloys; however, the output is still not sufficient. One drawback of Heusler-alloy-based CPP-GMR junctions is the "too small" junction resistance, which is reported to be on the order of 20 mΩ·μm$^2$ in *RA* values. According to simulations by Takagishi and co-workers, realizing the *optimal* junction resistance is necessary to overcome both spin-transfer torque and Joule heating problems.[1)] The spin-transfer torque problem defines the lower boundary of the *RA* values, because the magnetization is predicted to fluctuate for a small junction resistance under a large current density on the order of $10^8$ A/cm$^2$, which causes spin-transfer torque noise. In contrast, the Joule heating problem defines the upper boundary of the *RA* values. From the simulation of Takagishi et al., it is estimated that an MR ratio on the order of 70% is required for the *RA* values of the reported CPP-GMR junctions using Co-based full Heusler alloys and a Ag spacer layer. If the *RA* value is 50 mΩ·μm$^2$, the required value of the MR ratio is about 50% for an areal recording density of 5 Tbits/in.$^2$.[1)] Therefore, it is desirable to identify any new spacer material that increases the *RA* value without degrading the MR ratio value of Heusler-alloy-based CPP-GMR junctions.

Regarding investigations of spacer materials, several earlier experimental works used, for example, the non-magnetic Heusler alloy $Rh_2CuSn$,[11)] semiconductive wurtzite ZnO,[12)] *B*2 NiAl alloy,[13)] and In–Zn–O;[14)] however, none of those have yet been shown to be suitable for achieving the needed HDD specification of >5 Tb/in.$^2$.

Compared with ferromagnetic materials, spacer materials have not been investigated well. Thus, in this paper, we focus on an $L1_2$ Ag–Mg alloy as a new spacer material for the CPP-GMR junction to increase the $\Delta RA$ value. Ag–Mg alloys form the ordered $L1_2$ structure, which is called the $\alpha$ phase, for a relatively wide range of Mg compositions up to 25 at. %.[15,16)] Moreover, lattice mismatches between $L1_2$ $Ag_3Mg$ and Co-based full Heusler alloys are typically less than 3%, which is good for fabricating epitaxially grown heterojunctions. Concerning the transport properties, a higher resistivity was reported in a bulk sample compared with pure Ag,[15)] which potentially increases the *RA* value of the junction. Despite the lack of theoretical or experimental investigation of the CPP-GMR effect using Ag–Mg alloys, it is expected that the conduction electron spins are not scattered as much by the $L1_2$ Ag–Mg layer compared with the case of Ag-based CPP-GMR junctions because Mg is a relatively light element with small spin–orbit coupling.

All films were prepared by an ultrahigh-vacuum magnetron sputtering system (base pressure $<1 \times 10^{-7}$ Pa). The stacking structure for the CPP-GMR junction is MgO(100) substrate/Cr (20 nm)/Ag (40 nm)/$Co_2Fe_{0.4}Mn_{0.6}Si$ (20 nm)/Ag(–Mg) (5 nm)/$Co_2Fe_{0.4}Mn_{0.6}Si$ (7 nm)/Ag (2 nm)/Au (5 nm). All layers were deposited at room temperature, and post-annealing was performed at 650 and 500 °C after the deposition of Cr and the top $Co_2Fe_{0.4}Mn_{0.6}Si$ (CFMS) layer, respectively. The Ag–Mg layer was deposited by a co-sputtering process from Ag and Mg targets. The film composition was designed to be $Ag_{83}Mg_{17}$ (at. %), which was determined by inductively coupled plasma optical emission spectroscopy measurements. The structural properties of the Ag–Mg layer were characterized by reflection high-energy electron diffraction (RHEED). A sample using a Ag spacer was also prepared as a reference sample. The prepared films were patterned into a pillar shape using electron beam lithography and Ar ion dry etching. The designed junction sizes ranged from $50 \times 100$ nm$^2$ to $400 \times 800$ nm$^2$. Transport properties were measured by a direct current four-probe method at room temperature.

Figure 1(a) schematically illustrates the $L1_2$ $Ag_3Mg$ unit cell. A layered structure with alternate stacking of Ag–Mg and Ag planes is formed for the ⟨100⟩ azimuth of the $L1_2$ $Ag_3Mg$ alloy. Figures 1(b) and 1(c) show RHEED images of the Ag–Mg film surface at the ⟨100⟩ and ⟨110⟩ azimuths, respectively; the film was deposited onto an epitaxially

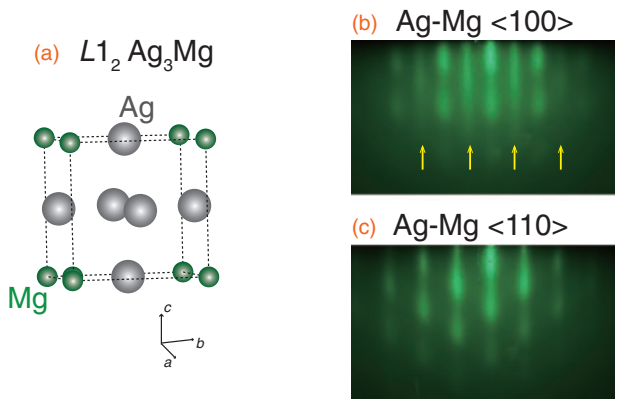


**Fig. 1.** (a) Unit cell of the $L1_2$ $Ag_3Mg$ alloy. RHEED patterns for the surface of Ag–Mg layer for azimuths of (b) Ag–Mg ⟨100⟩ and (c) Ag–Mg ⟨110⟩. Yellow arrows indicate superlattice diffraction from the $L1_2$-ordered structure.

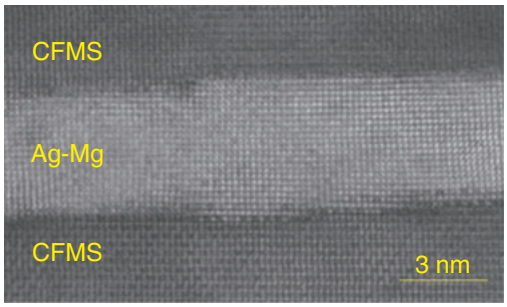


**Fig. 2.** Cross-sectional HAADF-STEM image of the CFMS/$Ag_{83}Mg_{17}$/CFMS junction.

grown CFMS(001) film prepared similarly to the bottom electrode of the CPP-GMR structure. Epitaxial growth of the Ag–Mg layer was confirmed from the RHEED pattern, and superlattice diffraction was also observed [as indicated by yellow arrows in Fig. 1(b)]. RHEED observation of the top CFMS surface was also performed for the samples of CPP junctions (data not shown here). The superlattice streak patterns associated with the $L2_1$ structure, as well as epitaxial growth of the CFMS layer, were confirmed.

Figure 2 shows a cross-sectional high-angle annular dark-field scanning transmission electron microscopy (HAADF-STEM) image around the CFMS/$Ag_{83}Mg_{17}$/CFMS interfaces of a film for the CPP-GMR junctions. The Ag–Mg spacer layer was found to have partially ordered $L1_2$ structure that exhibited pairs of periodic dark and light contrasts, especially around the CFMS/Ag–Mg interfaces. Concerning the structure of the CFMS layers, most parts showed clear contrasts representing $L2_1$ ordering of the Heusler alloy.

The size dependence of the junction resistance was examined to determine the values of *RA* and the parasitic resistance ($R_{para}$), as shown in Fig. 3. Each data point represents an average of 10 measurements. The data points show some deviation from the linear relationship for the Ag–Mg spacer junctions, especially for the $1/A$ values over $60\,\mu m^{-2}$, which can probably be attributed to the size distribution resulting from the electron lithography process in the relatively small junction area. Linear fitting was performed to estimate the *RA* values using nine data points

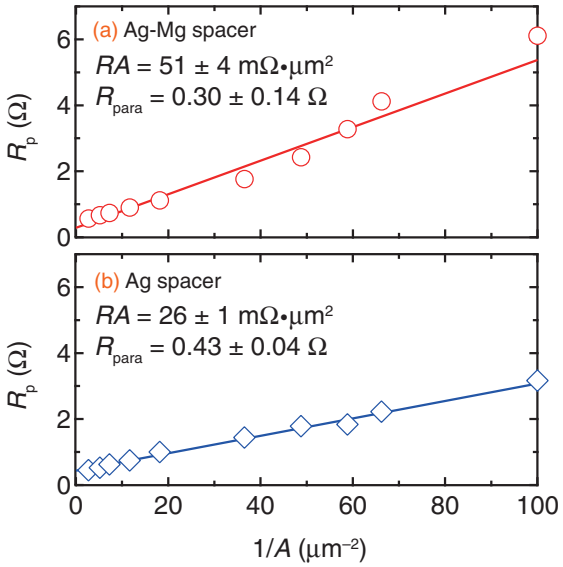


**Fig. 3.** Plots of the junction resistances in the parallel magnetization configuration ($R_p$) as a function of the inverse of the junction area ($1/A$) for (a) the Ag–Mg spacer and (b) the Ag spacer.

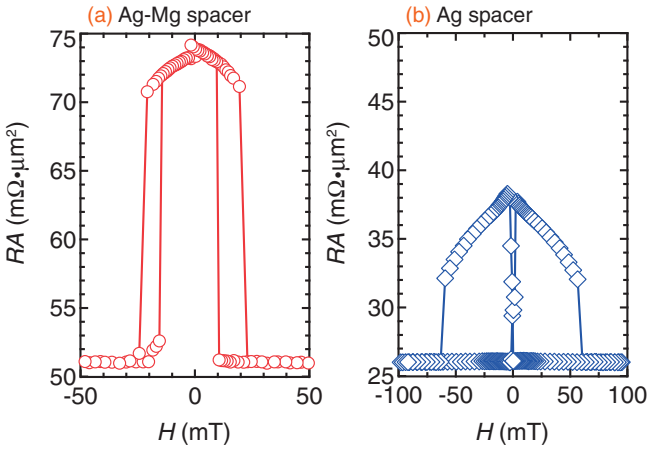


**Fig. 4.** Magnetoresistance curves of the CPP-GMR junctions using (a) the Ag–Mg spacer and (b) the Ag spacer.

with $1/A$ values below $70\,\mu m^{-2}$ for both spacer junctions. The estimated values of *RA* ($R_{para}$) were $51 \pm 4\,m\Omega{\cdot}\mu m^2$ ($0.30 \pm 0.14\,\Omega$) and $26 \pm 1\,m\Omega{\cdot}\mu m^2$ ($0.43 \pm 0.04\,\Omega$) for junctions using a Ag–Mg spacer and a Ag spacer, respectively. We also considered some other selections of data points for the linear fitting to eliminate possible overestimation of the *RA* values and confirmed that the values above are minimum estimations.

The MR curves are shown in Fig. 4. The vertical axes represent the *RA* values determined by eliminating the $R_{para}$ estimated in Fig. 3. Pseudospin valve-type curves were observed for both junctions, and the observed MR ratios ($MR_{obs}$), which include the $R_{para}$ value of the lead electrodes, were 40 and 38% for the Ag–Mg spacer [Fig. 4(a)] and the Ag spacer [Fig. 4(b)] junctions, respectively. The intrinsic value of the MR ratio ($MR_{int}$ ratio) was also deduced using the following equation:

$$MR_{int} \equiv \frac{\Delta R}{R_{junction}} = \frac{R_{AP} - R_P}{R_P - R_{para}}, \quad (1)$$

**Table I.** Summary of the specifications of the junctions investigated in this study. The observed value of the MR ratio ($MR_{obs}$) was defined as $MR_{obs} = (R_{AP} - R_P)/R_P$, where $R_P$ includes the parasitic resistance of the junction. $MR_{int}$ is defined by Eq. (1) in the main text. The values without brackets are the averages for $MR_{obs}$, $MR_{int}$, and $\Delta RA$, and those in the brackets are the maximum values for each quantity.

| Mg content (at. %) | $RA$ ($m\Omega{\cdot}\mu m^2$) | $MR_{obs}$ (%) | $MR_{int}$ (%) | $\Delta RA$ ($m\Omega{\cdot}\mu m^2$) |
|---|---|---|---|---|
| 0 | 26 | 35 (38) | 48 (54) | 13 (15) |
| 17 | 51 | 36 (40) | 44 (48) | 23 (25) |

where $R_{junction}$, $R_{AP}$, and $R_P$ represent the intrinsic junction resistance excluding $R_{para}$, the resistance in the antiparallel magnetization configuration, and that in the parallel configuration, respectively. The average deduced $MR_{int}$ ratios of the Ag–Mg spacer and the Ag spacer junctions were 44 and 48%, respectively. The average changes in the $RA$ values ($\Delta RA$) were also obtained as 23 and 13 $m\Omega{\cdot}\mu m^2$ for junctions using Ag–Mg and Ag spacers, respectively, and the maximum $\Delta RA$ value among the measured Ag–Mg spacer junctions was 25 $m\Omega{\cdot}\mu m^2$. The specification of the Ag–Mg spacer junction lies at the edge of that for HDD reading heads (a recording density of 5 Tbits/in.$^2$).[1] Table I summarizes the $RA$, $MR_{obs}$, $MR_{int}$, and $\Delta RA$ values of the junctions in this study.

Although the Ag–Mg spacer junctions exhibit slightly smaller values of $MR_{int}$ than the Ag spacer ones, $\Delta RA$ becomes much larger because of the larger value of $RA$ (which was nearly twice that of the Ag spacer junctions). According to the model of Valet and Fert,[10] $\Delta RA$ can be expressed as

$$\Delta RA = \frac{(2\beta\rho^*_{FM}t_{FM} + 2\gamma AR^*_{FM/NM})^2}{2\rho^*_{FM}t_{FM} + 2AR^*_{FM/NM} + 2\rho_{NM}t_{NM} + 2AR^*_{FM/NM}}, \quad (2)$$

where $\beta$, $\gamma$, $\rho^*_{FM}$, $\rho_{NM}$, $t_{FM(NM)}$, and $R^*_{FM/NM}$ represent the bulk spin asymmetry coefficient, the interface spin asymmetry coefficient, the spin resistivity of the ferromagnetic layer, the resistivity of the nonmagnetic spacer, thickness of the ferromagnetic (nonmagnetic) layer, and the interface resistance at the ferromagnetic/nonmagnetic interface, respectively. Equation (2) is valid in the limit in which the thickness of the ferromagnetic layers and the nonmagnetic spacer is shorter than the spin diffusion length. From Eq. (2), we qualitatively propose that a possible reason for the enhanced $\Delta RA$ value of the Ag–Mg spacer junctions is an increase in $R^*_{FM/NM}$ [$\equiv R_{FM/NM}/(1-\gamma^2)$], because if the increase in $RA$ was caused only by the increase in $\rho_{NM}$, $\Delta RA$ would decrease according to Eq. (2). In addition, the $RA$ value for the Ag–Mg junction cannot be explained by the resistivity value for the disordered Ag–Mg alloy nor by the reported value for the $L1_2$-ordered Ag–Mg alloy in Ref. 15. The reason is that the $RA$ values of the 5-nm-thick spacer materials estimated from the bulk resistivity values are about $8 \times 10^{-2}$ and $25 \times 10^{-2}$ $m\Omega\,\mu m^2$ for Ag and $L1_2$ $Ag_3Mg$, respectively, which are much smaller than the experimental values. According to theoretical studies, for example, the predictions in Refs. 17 and 18, it is essential to choose a ferromagnetic material and a nonmagnetic spacer material with good band-matching for fabricating high-output CPP-GMR junctions. Although a theoretical investigation is outside the framework of this paper, the dispersion relation of $L1_2$ $Ag_3Mg$[19] is completely different from that of face-centered cubic Ag,[20] which possibly modifies the band-matching between CFMS and the spacer layer.

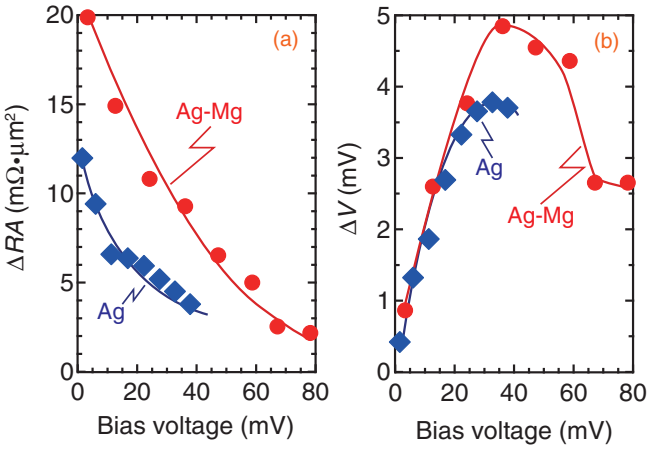


**Fig. 5.** Bias voltage dependence of (a) $\Delta RA$ and (b) output voltage $\Delta V$ for the CPP junctions. Red solid circles and blue solid diamonds represent data points for the junctions using the Ag–Mg spacer and the Ag spacer, respectively.

Finally, the bias voltage dependence of $\Delta RA$ and the output voltage ($\Delta V$) was investigated for CPP-GMR junctions, as shown in Figs. 5(a) and 5(b), respectively. Here, $\Delta V \equiv \Delta R \times I_{bias} = (R_{AP} - R_P) \times I_{bias}$, where $I_{bias}$ represents the measured bias current. The maximum applied current was 14 mA, corresponding to a current density ($J$) of about $10^8$ A/cm$^2$ at 78 and 38 mV for the $L1_2$ Ag–Mg and Ag spacer junctions, respectively. With increasing bias voltage, $\Delta RA$ decreases monotonically, which is attributed to fluctuation of the magnetization vectors due to spin-transfer torque and Joule heating. The maximum values of the output voltage ($\Delta V$) are 4.8 and 3.8 mV for the Ag–Mg and Ag spacer junctions, respectively. These results indicate an advantage of the Ag–Mg spacer layer over the Ag spacer one for application to the reading head element of HDDs.

In summary, CPP-GMR effects were investigated in CFMS/$Ag_{83}Mg_{17}$/CFMS junctions. An epitaxially grown multilayer sample was fabricated with an $L1_2$-ordered $Ag_{83}Mg_{17}$ spacer layer and $L2_1$-ordered CFMS ferromagnetic layers. The average observed (intrinsic) values of the MR ratio were 36% (44%) and 35% (48%) for the junctions using $Ag_{83}Mg_{17}$ and Ag spacers, respectively. The $RA$ value for the Ag–Mg spacer junction was 51 $m\Omega{\cdot}\mu m^2$, which is twice that of the Ag spacer junction. Owing to the large $RA$ value, a $\Delta RA$ value of 25.2 $m\Omega{\cdot}\mu m^2$ was achieved for the Ag–Mg spacer junction at maximum. The output voltage for the Ag–Mg spacer junction was 4.8 mV at a bias voltage of 38 mV, which is also larger than that for the Ag spacer. Those experimental results suggest that CPP-GMR junctions using a Ag–Mg spacer layer would be advantageous for use in the reading head of HDDs.

**Acknowledgments** This work was partially supported by the Foundation for Promotion of Material Science and Technology of Japan; the Hattori Hokokai Foundation; the ImPACT program of the Council for Science, Technology and Innovation (Cabinet Office, Government of Japan); and a Grant-in-Aid for Scientific Research (No. 25220910) from the Japan Society for the Promotion of Science (JSPS). A part of this work was done through a cooperative program (Proposal No. 14G0412) of the Cooperative Research and Development Center for Advanced Materials, Institute for Materials Research, Tohoku University.

1) M. Takagishi, K. Yamada, H. Iwasaki, H. N. Fuke, and S. Hashimoto, IEEE Trans. Magn. **46**, 2086 (2010).
2) S. Ishida, S. Fujii, S. Kashiwagi, and S. Asano, J. Phys. Soc. Jpn. **64**, 2152 (1995).
3) K. Yakushiji, K. Saito, S. Mitani, K. Takanashi, Y. K. Takanashi, and K. Hono, Appl. Phys. Lett. **88**, 222504 (2006).
4) T. Iwase, Y. Sakuraba, S. Bosu, K. Saito, S. Mitani, and K. Takanashi, Appl. Phys. Express **2**, 063003 (2009).
5) T. Furubayashi, K. Kodama, H. Sukegawa, Y. K. Takahashi, K. Inomata, and K. Hono, Appl. Phys. Lett. **93**, 122507 (2008).
6) T. M. Nakatani, S. Mitani, T. Furubayashi, and K. Hono, Appl. Phys. Lett. **99**, 182505 (2011).
7) J. Sato, M. Oogane, H. Naganuma, and Y. Ando, Appl. Phys. Express **4**, 113005 (2011).
8) Y. Sakuraba, M. Ueda, Y. Miura, K. Sato, S. Bosu, K. Saito, M. Shirai, T. J. Konno, and K. Takanashi, Appl. Phys. Lett. **101**, 252408 (2012).
9) S. Li, Y. K. Takahashi, T. Furubayashi, and K. Hono, Appl. Phys. Lett. **103**, 042405 (2013).
10) T. Valet and A. Fert, Phys. Rev. B **48**, 7099 (1993).
11) K. Nikolaev, P. Kolbo, T. Pokhil, X. Peng, Y. Chen, T. Ambrose, and L. Mrysaov, Appl. Phys. Lett. **94**, 222501 (2009).
12) K. Shimazawa, Y. Tsuchiya, T. Mizuno, S. Hara, T. Chou, D. Miyauchi, T. Machita, T. Ayukawa, T. Ichiki, and K. Noguchi, IEEE Trans. Magn. **46**, 1487 (2010).
13) N. Hase, T. M. Nakatani, S. Kasai, Y. K. Takahashi, T. Furubayashi, and K. Hono, J. Magn. Magn. Mater. **324**, 440 (2012).
14) T. Nakatani and J. R. Childress, 59th Annu. Conf. Magnetism and Magnetic Materials, 2014, CG-05.
15) K. Fujiwara, M. Hirabayashi, D. Watanabe, and S. Ogawa, J. Phys. Soc. Jpn. **13**, 167 (1958).
16) Alloy Phase Diagram, Diagram No. 1201632, 1998.
17) Y. Sakuraba, K. Izumi, T. Iwase, S. Bosu, K. Saito, K. Takanashi, Y. Miura, K. Futatsukawa, K. Abe, and M. Shirai, Phys. Rev. B **82**, 094444 (2010).
18) V. Ko, G. Han, and Y. P. Feng, J. Magn. Magn. Mater. **322**, 2989 (2010).
19) O. l. Velikokhatnyi, S. V. Eremeev, I. I. Naumov, and A. I. Potekaev, J. Phys.: Condens. Matter **12**, 8825 (2000).
20) A.-B. Chen and B. Segall, Phys. Rev. B **12**, 600 (1975).